[PROC. OF JSCE No. 418/III-12 (Geotechnical Eng.) June 1990]

UNDRAINED STABILITY OF TWO-DIMENSIONAL UNLINED TUNNELS IN SOFT SOIL

By Jiro TAKEMURA, Tsutomu KIMURA** and Sing Fang WONG****

The paper presents the results of centrifuge model tests and upper bound calculations on two-dimensional unlined tunnels in two different normally consolidated cohesive soils with the plasticity index of 10 and 25. The upper bound calculations were carried out by taking the variation of soil strength with depth and the strength anisotropy into account. It is found that the undrained stability of the tunnels increases with increasing tunnel cover-to-diameter ratio and that observed surface settlement profiles are different for the two soils. The critical tunnel pressures as well as the collapse mechanisms deduced from the bound calculation compare well with the observations. It is confirmed that the surface settlement profiles can be represented by the error functions fairly accurately.

Keywords: *two dimensional tunnel, stability, soft clay, model test, upper bound*

1. INTRODUCTION

In the last two decades, replying to the urgent need for the construction of infra-structures, shield tunnelling has been conducted widely in urban areas. Although the technique has been advanced recently owing to the accumulation of practical experiences and the progress in the mechanical sides, there still remain many unknown problems especially in soft ground tunnelling.

For tunnelling in soft ground one must always consider not only the stability of a tunnel itself but also the surface settlement due to deformations of soil around the tunnel. Although the patterns of the surface settlements differ for different soil conditions and methods of tunnelling, many field observations[1),2)] and model tests[3)~5)] show that the troughs of surface settlement can be approximated by the error functions or Gaussian normal distribution curves. One way of describing the settlement troughs is to use a parameter i/D, where i is the standard deviation of the error function, and D is the tunnel diameter shown in Fig. 1 (c). This parameter depends on the cover or the depth of tunnel C and the type of soil[1),3),4)]. From model tests on overconsolidated kaolin and loose and dense sands, Atkinson *et al.*[3)] reported that the ratio S_{max}/S_c depends on the ratio C/D and surcharge pressure p_0, where S_{max} is the maximum surface settlement or mid-surface settlement and S_c the crown settlement. This is supported by field observations[2)]. On the contrary, centrifuge model tests on kaolin carried out by Taylor[5)] showed that the S_{max}/S_c is independent of C/D and that S_{max} and S_c depend on the load factor which is defined as the ratio of current stability ratio N_c to that at tunnel collapse. The stability ratio was first defined as $(\sigma_T-\sigma_S)/c_u$ by Broms and Bennermark[6)], where σ_T is the total overburden pressure at the depth of tunnel axis, σ_S the

* Member of JSCE, M. Eng., Research Associate, Dep. Civil Eng., Tokyo Institute of Technology (Ookayama Meguro-ku Tokyo)
** Member of JSCE, Dr. Eng., Professor, Dep. Civil Eng., Tokyo Institute of Technology (Ookayama Meguro-ku Tokyo)
*** Penta Ocean Construction (Singapore)

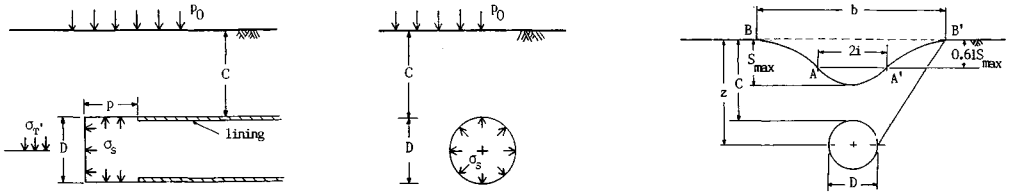

(a) Three dimensional problem. (b) Two dimensional problem (c) Profile of surface settlement

Fig. 1

tunnel support pressure and c_u the undrained shear strength. For undrained and plane strain conditions, the volume of ground lost in the tunnel per unit length is equal to the area of the surface trough. Based on the results of centrifuge tests on overconsolidated kaolin and finite element analyses, Mair *et al.*[4] concluded that ground loss is better related to the load factor than the stability ratio.

In addition to the factors mentioned above, there are many other factors influencing the movements in soft soil around tunnels. Many research workers and engineers found that such factors as the methods of tunnelling, the excavation ratio[7], the duration between excavation and lining[8),9], the distance from the tunnel face to the structural lining p[10] (Fig. 1 (a)) and disturbance of soil around tunnels[11] determine the soil deformations.

The stability of the tunnel itself is also determined by factors similar to those related to the deformations. From a series of tests in which clay was forced through a cylindrical hole, Broms and Bennermark[6] concluded that the undrained stability of tunnels depends only on the stability ratio N_c. Field data support the conclusion[1),12] and centrifuge model tests by Mair[13] give similar results for shallow tunnels. Mair also showed that N_c decreases with the increase of the ratio p/D (Fig. 1 (a)) and that unlined two-dimensional tunnels are less stable than partially unlined three-dimensional tunnels. It has been found that the bound calculation based on appropriate failure mechanisms can predict the results of model tests reasonably well[10),14].

Great many research works have been carried out on shallow tunnelling. It seems, however, that researches on tunnelling in very soft soil, especially in normally consolidated clay which usually has very low strength at the surface with the strength increasing linearly with depth, have not yet been conducted properly. This is probably because there is a considerable difficulty in creating such strength profile in a clay of a small model under gravity or 1 g field. It has been found that this type of clay can be prepared fairly easily by using a centrifuge even in a small model[15]. The usefulness of centrifuge modelling in investigating the phenomena governed by the self-weight of soil like tunnel collapse has been appreciated by several research workers[5),13),16].

In this study, a series of centrifuge model tests on two-dimensional shallow tunnels with C/D ranging from 1.0 to 3.0 in two different normally consolidated cohesive soils were carried out to investigate the undrained stability and the deformations around the tunnels. Upper bound calculations were conducted taking the strength anisotropy of the soils into account. The results of the analyses are compared with those of the model tests.

2. CENTRIFUGE MODEL TESTS

(1) Soils

Two artificial cohesive soils prepared from an identical Kawasaki clay with plasticity index, (I_p), of 40 were used in the centrifuge model tests. The soil mechanics group of Tokyo Institute of Technology has carried out extensive researches on these artificial soils in order to study the mechanical behaviour of intermediate soils[17)~19]. It was found that the mechanical properties including strength anisotropy of the mixtures with I_p greater than 20 are similar to those of the original clay, but that the mixtures with I_p less than 15 exhibit different characteristics[19]. The plasticity indices of the soil used in the model tests were

about 10 and 25. In this tests they are named M-10 and M-25 referring to their plasticity index respectively. The index and mechanical properties of each soil are listed in Table 1.

(2) Test system

Mark II centrifuge of Tykyo Institute of Technology was used in the tests. Its specifications and details were described by Kimura *et al.* [18].

The test system is schematically illustrated in Fig. 2. The internal dimensions of the centrifuge strong box are 480 mm in length, 200 mm in breadth and 320 mm in height. The box consists of three parts ; a front wall, a rear wall and a main frame made by welding together two side and one base plates. The three parts are joined together by bolts. The front wall has a 32 mm thick Lexan sheet fixed to a steel frame. There is an acrylic screw in the Lexan sheet to be used for drilling a tunnel. On the rear wall there is also a steel plug having a hole of 45 mm in diameter for tunnel cutting. There are holes on the rear wall for insertion of pore pressure transducers. In order to control the drainage conditions at the bottom, synflex tubes connected to the bottom drainage layer were joined to two solenoid valves. A rubber bag of 40 mm in diameter, 205 mm in length and 0.5 mm in thickness was used for modelling an unlined tunnel. Synthetic fibers are laid inside the rubber so that the bag has considerable resistance against expansion.

On top of the soil block was a thin layer of lead shot for applying surcharge pressure during centrifugation. The surface settlements and pore water pressures were measured by LVDTs mounted on the box and pore pressure transducers embedded in the soil respectively. Deformations of the soil were traced by observing the movements of optical targets placed across the front of the soil (Fig. 2) using a photographic camera. The positions of LVDTs and pore pressure transducers are shown in Fig. 3.

(3) Test procedures and conditions

Test procedures are divided into three steps ; sample preparation, model preparation and tunnel test. The details of the procedures are as follows.

a) Sample preparation

The soils were remoulded at water contents of twice their liquid limits. Slurry was deaired under a negative pressure of about −90 kPa for half an hour and poured into the strong box. Prior to pouring of the slurry, the bottom drainage layer was made by compacting coarse silica sand to a thickness of 20 mm. Subsequently silicone grease was smeared onto the inner faces of the box to reduce the side friction.

Table 1 Properties of soils.

		M-10	M-25
Liquid limit LL (%)		27.4	46.0
Plastic limit PL (%)		17.7	23.4
Plasticity Index I_p		9.7	22.6
Specific gravity of soil particles G_s		2.67	2.68
Oedometer test	Compression Index C_c	0.117	0.224
	Void ratio at 98kPa $(c_u/p)K_0$	0.380	0.395

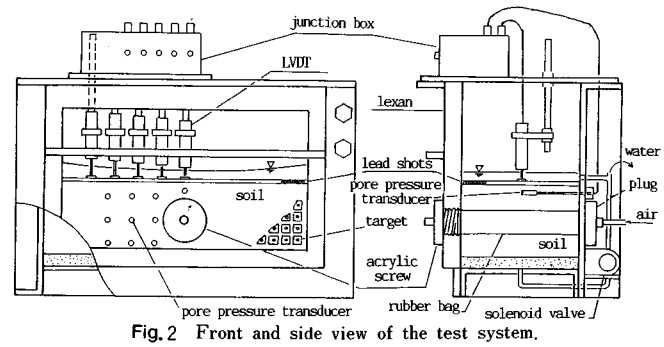

Fig. 2 Front and side view of the test system.

Table 2 Test conditions and measured C/D ratios.

Test code	Soil	Tunnel diameter D (mm)	C/D Specified	C/D Measured	Surcharge pressure p_0 (kPa)
T121	M-10	40	1.0	1.13	20
T135	M-10	40	1.5	1.57	20
T142	M-10	40	2.0	2.19	20
T167	M-10	40	3.0	3.04	20
T224	M-25	40	1.0	1.01	20
T236	M-25	40	1.5	1.50	20
T243	M-25	40	2.0	2.00	20

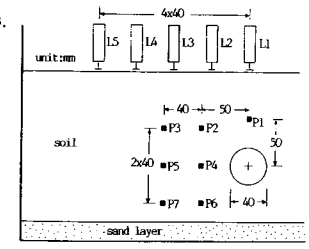

Fig. 3 Positions of LVDTs and pore pressure transducers.

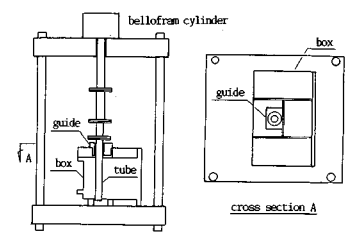

Fig. 4 Tunnel cutting equipment.

Preconsolidation was carried out by pressing down a rigid loading plate with a bello-fram cylinder on the lab floor. The preconsolidation pressure at the first stage was three quarters of the surcharge pressure p_0 in the centrifuge tests, i. e. 15 kPa.

On completion of the preconsolidation, the optical targets were placed and seven pore pressure transducers were inserted into the sample. The second stage-preconsolidation was carried out on the lab floor under a pressure of 20 kPa which is identical to p_0.

b) Model preparation

After having completed consolidation on the lab floor the surface of the sample was shaped to a thickness a few mm greater than the specified value allowing for the settlement due to subsequent centrifugal consolidation. The specified tunnel cover-to-diameter ratios for each test are shown in Table 2. A thin sheet of gauze was then laid on the surface and lead shot with 2 mm in diameter was evenly spread over it. At the centrifugal acceleration of 60 g, the pressure acting on the surface due to the lead shot was nearly equal to the surcharge pressure p_0. A row of 5 LVDTs were installed on the surface and finally the weight of the system was measured.

After mounting the strong box and counter-weights onto each end of the centrifuge, centrifugal acceleration was increased up to 60 g in 10 g increments. During the centrifugal consolidation under 60 g, pore pressures and settlements were recorded to monitor the progress of consolidation. The time required for achieving 90 % consolidation was about 6 to 37 hours, which depended on the type of soil and the thickness of the sample.

Confirming 90 % consolidation by the square root t method for the settlement of the center of the sample, two solenoid valves connected to drainage tubes were shut off to prevent water from flowing back into the sample. Centrifuge was then stopped and the strong box was taken out. The LVDTs, lead shot and acryl screw on the front wall were removed and the box was laid down horizontally on the tunnelling platform with its rear wall facing upwards as shown in Fig. 4. The plug was removed from the rear wall and a tunnelling guide was fixed to the wall.

Tunnel cutting was performed by pushing a thin walled steel tube with 40 mm in outer diameter into the sample along the guide with a bello-fram cylinder. After pulling out the tube, a well-greased rubber bag was inserted into the tunnel and the plug was put back. The front screw, lead shot and LVDTs were put back into their positions and then centrifugation was conducted again.

c) Tunnel test

Centrifuge acceleration was increased up to 60 g in 5 g increments. At each step air pressure in the bag was adjusted to the tunnel supporting pressure σ_S so that no appreciable deformations would take place in the surrounding soil. Although the block of soil which was consolidated in K_0 condition was subjected to some deformations due to tunnel cutting, the stress condition in the soil is considered to be still very close to that in K_0 consolidation. The calculated redial stresses around the tunnel are shown in Fig. 5 where K_0 was taken as 0.45. As it was not possible to determine the actual tunnel supporting pressure from these complicated stresses, the total vertical pressure at the crown which is 2 % to 20 % higher than the average value of the radial stresses in this test series was selected as an alternative.

The models were left in the 60 g field for about 30 to 60 minutes until the settlement increment per minute at the center of the surface became less than 0.01 mm. The solenoid valves were then shut off and the tunnel test was performed by reducing the air pressure in the rubber bag in decrements of 10 kPa for every 30 seconds. Two photographs were taken at each step while air pressure in the bag, pore water pressures and settlements on the surface were recorded continuously by a data recorder. Seven tests were carried out as shown in Table 2, in which actual C/D ratios measured from the photographs taken before each tunnel test are also given. The first number of the test code refers to the name of the soil used; "1" for M-10 and "2" for M-25, a half of the second number gives the C/D ratio and the third is the serial number of the tests. In tests T135 and T236 an attempt was made to measure the settlements of tunnel crown by a

non-contact type displacement transducer embedded inside the rubber bag. Each test lasted for about 5 to 7 minutes.

3. RESULTS AND DISCUSSIONS

(1) Stability of tunnels

Typical variations of surface settlements with tunnel pressures for two types of soils, T142 and T243, are given in Fig. 6. The codes in the figure refer to the positions of LVDTs shown in Fig. 3. Settlements develop slowly at the initial stages and increase suddenly when the tunnel pressure was reduced beyond a certain value. At the final stages when only little changes in the settlement were observed, the tunnel is considered to have completely collapsed. With respect to the curve of the settlements of mid-suface labeled as L1 in Fig. 6, the maximum curvature and the steepest straight portion appear near the point of 1 mm settlement and just before the very final stage respectively.

For tests T135 and T236, the tunnel crown settlements S_c are plotted against the mid-surface settlements S_{max} in Fig. 7. The crown settlements progress at the rate of nearly twice that of mid-suface settlements until S_c amounts to about 1.6 mm, indicating that the soil mass above the crown is in the state of extension. After this the rate for S_c becomes nearly equal to that for S_{max}, implying that the soil mass above the crown moves as a block. This particular settlement corresponds roughly to the settlement at which the maximum curvature appears in the curve L1 in Fig. 6.

The critical tunnel pressure, at which tunnels collapse, is important in discussing the stability of unlined tunnels. Since it was rather difficult to determine the critical tunnel pressure from the results of the tests, the authors attempt to discuss the stability using two prominent pressures on the settlement-tunnel pressure curve. One is the pressure at which the settlement of mid-surface is equal to 1 mm, and the other is that at the onset of the steepest straight portion in the same curve marked by an arrow. It might be said that the former is the upper limit of critical tunnel pressure and the latter is the lower limit. In Table 3 the effective critical tunnel pressures σ'_c obtained by subtracting the hydrostatic pressures at tunnel axis from the observed critical tunnel pressures are given together with stability ratios N_c calculated from σ'_c. The equation for converting σ'_c into N_c will be explained later. The term "effective" adopted here has nothing to do with the conventional effective stress. It is simply the difference between the observed tunnel pressure and hydrostatic pressure. The authors consider the use of this "effective" pressure convenient because it gives more direct understanding of the variation of critical tunnel pressure with the depth of tunnel.

The effective critical pressures are plotted against the measured C/D ratios in Fig. 8. There is no significant difference between the results for the two soils. The critical pressure decreases with the increase of C/D and become negative at high values of C/D. This stress condition encourages water in soil to flow towards the tunnel, resulting in reduction in the undrained strength of soil around the tunnel due to swelling. This has to be born in mind when the long term stability of the tunnel is discussed.

It has been known that the upper bound calculation is a useful method to estimate the undrained stability

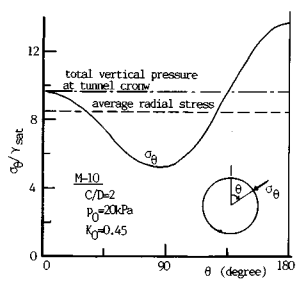

Fig. 5 Radial stresses around the tunnel.

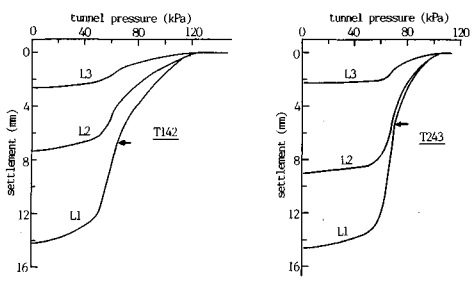

Fig. 6 Observed variations of surface settlement with tunnel pressure.

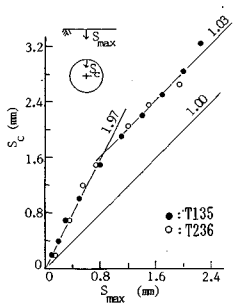

Fig. 7 Relationship between crown and mid-surface settlement.

Table 3 Results of failure tests.

Test code	hydrostatic pressure at tunnel axis (kPa)	effective overburden pressure at tunnel axis: σ_T' (kPa)	upper critical pressure		lower critical pressure	
			σ_c' (kPa)	stability ratio Nc	σ_c' (kPa)	stability ratio Nc
T121	44.1	54.9	25.9	1.39	3.9	2.40
T135	55.9	66.6	22.1	1.79	3.1	2.51
T142	67.6	78.4	38.4	1.34	-3.1	2.74
T167	91.1	102.0	31.9	1.81	-20.1	3.15
T224	44.1	48.5	22.9	1.34	10.4	1.99
T236	55.9	58.1	19.1	1.70	4.1	2.35
T243	67.6	67.8	23.4	1.66	1.4	2.48

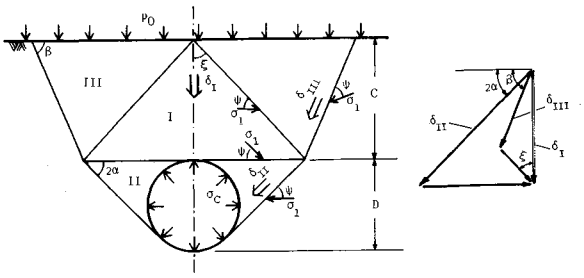

Fig. 9 Collapse mechanism and displacement diagram.

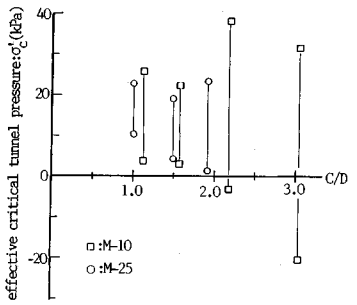

Fig. 8 Relationship between observed critical tunnel pressures and cover-to-diameter ratios (C/D).

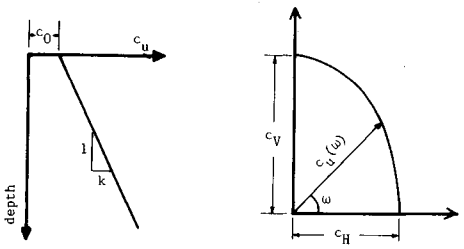

Fig. 10 Strength profile with depth and strength anisotropy.

of tunnels. In this study the authors attempt to carry out the upper bound calculations by incorporating the variation of the strength of clay and compare the results with the observations. The collapse mechanism was determined by referring to the observed deformations shown later. It consists of five rigid blocks with two variables, α and β, as shown in Fig. 9. The displacement diagram is also shown in the figure.

In the process of reduction of tunnel pressures, clay above the tunnel experiences extension as mentioned earlier. It has been reported that the extension strengths of intermediate soils are found to be less than the compression strengths and that the extension strengths are smaller for soils with lower plasticity index[19]. This strength anisotropy was also incorporated into the upper bound calculations by employing following assumptions;

1) The strength $c_u(\omega)$, with the major principal stress inclined at an angle ω with the horizontal, can be expressed by

$$c_u(\omega)=c_H+(c_V-c_H)\sin^2\omega \quad \cdots\cdots (1)$$

where c_H and c_V denote the strengths when the major principal stress is horizontal and vertical respectively. These strengths can be obtained from undrained triaxial extension and compression tests.

2) The ratio c_H/c_V is constant for a given soil and is denoted by m. The value of m is equal to unity in the isotropic stress condition.

3) The strength of clay at depth z is given by

$$c_V(z)=c_{0V}+k\cdot z \quad \cdots\cdots (2)$$

where c_{0V} denotes the value of c_V at the surface and k the gradient of the strength with respect to the depth. They are calculated from the following equations;

$$c_{0V}=p_0\cdot(c_u/p) \quad \cdots\cdots (3)$$

$$k=n\gamma'\cdot(c_u/p) \quad \cdots\cdots (4)$$

where c_u/p is the ratio of undrained strength to consolidation pressure, n centrifugal acceleration ratio, and γ' submerged weight of soil.

4) The unit weight of each soil is constant and calculated from the consolidation properties listed in Table 1 and surcharge pressure p_0.

5) The angle between the failure plane and the direction of the major principal stress, which is denoted by Ψ, is constant and can be taken as 45° considering undrained conditions.

The variation of soil strength with depth z and with the inclination of major principal stress are shown in Fig. 10.

The upper bound for critical tunnel pressure σ'_{cu} can be determined by equating the rate of external work done by the surcharge, tunnel pressure and the self-weight of soil to the rate of energy dissipated along the failure planes. The upper bound is given by the following equation ;

$$\begin{aligned}\sigma'_{cu}-p_0=&C\gamma'+\frac{D\gamma'}{2}\left\{1-\left(\frac{\pi}{2}-\alpha\right)\tan\alpha\right\}\\&-c_{ov}\left[\frac{1}{\sin 2\alpha}\{1-(1-m)\sin^2(\Psi+\alpha)\}+\frac{1}{\tan 2\alpha}\{1-(1-m)\cos^2\Psi\}\right.\\&\left.+\frac{2C\tan\alpha}{D\cos(\beta-\xi)}\left\{\frac{\cos\beta}{\cos\xi}\{1-(1-m)\sin^2(\Psi+\xi)\}+\frac{\sin\xi}{\sin\beta}\{1-(1-m)\sin^2(\Psi+\beta)\}\right\}\right]\\&-k\left[\left\{\frac{D}{4\tan\alpha}+\frac{C}{\sin 2\alpha}\right\}\{1-(1-m)\sin^2(\Psi+\alpha)\}+\frac{C}{\tan 2\alpha}\{1-(1-m)\cos^2\Psi\}\right.\\&\left.+\frac{C^2\tan\alpha}{D\cos(\beta-\xi)}\left\{\frac{\cos\beta}{\cos\xi}\{1-(1-m)\sin^2(\Psi+\xi)\}+\frac{\sin\xi}{\sin\beta}\{1-(1-m)\sin^2(\Psi+\beta)\}\right\}\right]\end{aligned}\quad\cdots\cdots(5)$$

where $\xi=\tan^{-1}\left\{\dfrac{D}{2C\tan\alpha}\right\}$

As there involve no volume changes under undrained conditions, the decrease in the area of tunnel must equal the ground loss. The best upper bound solution is obtained from above equation as the maximum value by varying the angles α and β.

In this test series, the stability ratio N_c, defined by Broms and Bennermark[6], is expressed by

$$N_c=\frac{\sigma'_T-\sigma'_c}{c_{uT}}=\frac{p_0+n\gamma'\left(C+\frac{1}{2}\right)D-\sigma'_c}{\left\{p_0+n\gamma'\left(C+\frac{1}{2}\right)D\right\}(c_u/p)}\quad\cdots\cdots(6)$$

where c_{uT} is the undrained strength at the tunnel axis. The values of N_c calculated by Eq. (6) using observed σ'_c are listed in Table 3, and plotted against the measured C/D ratios together with the calculated upper bounds in Fig. 11. Nakase and Kamei[19] reported that the strength ratio m for the K_0 consolidated specimens of artificial mixtures constituted from Kawasaki clay ranges from 0.5 for M-10 to

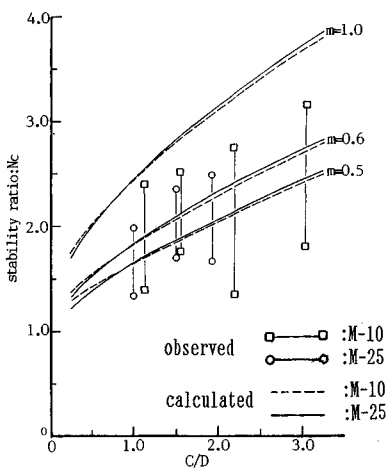

Fig. 11 Relationship between stability ratios (N_c) and cover-to-diameter ratios (C/D).

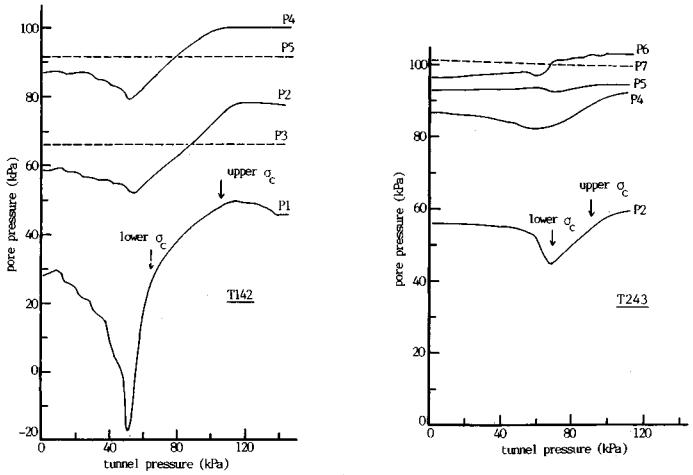

Fig. 12 Observed variations of pore pressures with tunnel pressures.

0.6 for clay with I_p greater than 20. Therefore the calculation was conducted for three different values of m i.e. 0.5, 0.6 and 1.0, for each soil. It can be said from the figure that the undrained stability of tunnels increases with the increase of C/D. The relationship between N_c and the ratio C/D for the same value of m are almost identical irrespective of soil type. In this test series, the difference in soil type is reflected only in γ' because c_u/p is nearly identical for the two soils and p_0 was constant in every test. The calculated tunnel pressures are different for the two soils, but, when they are converted into N_c, the difference becomes negligible as the effect of γ' cancels out. Although the stability ratio for M-10 with smaller m is expected to be lower than that for M-25, any significant difference was not found in the tests. The calculated N_c for m equal to 0.5 and 0.6 are in between N_c obtained from the measured lower and upper critical tunnel pressures, while those for m equal to 1.0 are greater than the observations. This leads to a conclusion that the strength anisotropy must be taken into account in the estimation of the undrained stability of tunnels.

The variations of pore pressures with tunnel pressures during tunnel tests T142 and T243 are illustrated in Fig. 12. The codes in the figure correspond to the positions of pore pressure transducers shown in Fig. 3. The pore pressure above the tunnel crown was not successfully measured in T243. Except for transducers that are more than 2 D away from the tunnel center, all the results indicate drops in pore pressures from a pressure somewhat larger than the upper critical tunnel pressure. Several field measurements around tunnels show a similar drop in pore pressures when part of the tunnel began to fail[20]. It is interesting to note that at the early stages of tunnel pressure reduction, pore pressures of M-10 tend to rise while those of M-25 tend to fall. This is consistent with the results of triaxial extension tests that M-10 exhibits higher positive pore pressures than soils with higher I_p in the beginning of the tests[19]. It is known that the existence of pore pressure gradient gives rise to local migration of water even in undrained conditions. At the early stages of the tunnel tests, therefore, water migrates away from the block of soil above the tunnel in M-10, causing local consolidation. On the contrary, in M-25 water flows into the block, causing swelling. As a result of this possible water migration, minor changes in the strength can take place for the two soils ; namely an increase for M-10 and a decrease for M-25. This change is considered to have masked the effect of m, yielding nearly the same N_c values in the tests as shown in Fig. 11.

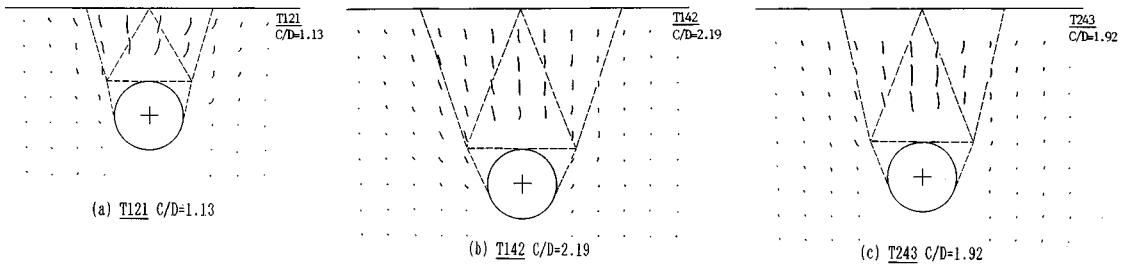

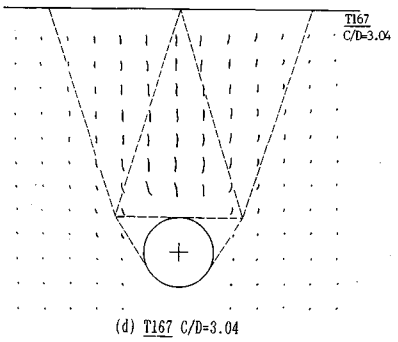

Fig. 13 Observed deformations and collapse mechanisms obtained from upper bound calculation.

Table 4 Observed parameters describing surface settlement.

Test code	S_{max} (mm)	$0.61S_{max}$ (mm)	$2i$ (mm)	b (mm)
T121	13.2	8.0	83	200
T135	7.9	4.8	65	189
T142	6.8	4.2	140	325
T167	7.2	4.4	129	381
T224	12.8	7.8	40	200
T236	10.3	6.3	45	166
T243	9.4	5.7	64	313

(2) Deformations

Observed deformations in tests T121, T142, T167 and T243 are shown in Fig. 13 together with the collapse mechanisms for the maximum critical tunnel pressure in the upper bound calculation in which the ratio m was taken as 0.5 for M-10 and 0.6 for M-25. In all the cases the soil mass above the tunnel moves almost vertically downwards. Soil that is slightly away from the tunnel tends to move towards the tunnel at a small angle. Large deformations occur only inside areas covered by the collapse mechanisms and directions of movement agree reasonably well with those in the mechanisms. This implies that the collapse mechanism used in the calculation is appropriate and that the obtained upper bound critical pressures should be close to the actual values.

Comparing the deformations for T142 and T243 with almost identical C/D, it is noticed that large deformations in T243 appear in a rather limited area. This corresponds to the results of the upper bound calculation that a higher value was obtained for β for T243 than for T142. A similar trend is found for another set of two tests with identical C/D. The difference in soil type seems to be reflected more markedly in the deformations than in the stability ratio.

Peck[1] showed that the profiles of surface settlements or settlement troughs can be approximated by the error function as given by

$$\frac{S(x)}{S_{max}}=\exp\left(-\frac{x^2}{2i^2}\right) \qquad (7)$$

in which i is the standard deviation of the error function or the distance form the centre-line to the point of inflection as shown in Fig. 1 (c). Fig. 14 shows the settlement profiles at the final stages of tunnel tests on two sets of geometrically similar models, i. e. T121 versus T224 and T142 versus T243. The surface settlement at the point of inflection is calculated as 0.61 S_{max} from Equation (7). The values of S_{max} and 2 i can be read off from the settlement curves in Fig. 14. These values specify the error function in Equation (7) and they are drawn in Fig. 14. These curves compare fairly well with the test results especially near the centre-line of the tunnel.

The surface settlement profiles can be expressed by a set of parameters ; S_{max}, 2 i and b shown in Fig. 1 (c). These parameters obtained from the observed profiles at the final stages of tunnel tests are given in Table 4. The width b normalized by the tunnel diameter D is plotted against z/D in Fig. 15, in which z is the depth from the ground surface to the tunnel axis and expressed as $C+D/2$. The ratio b/D increases

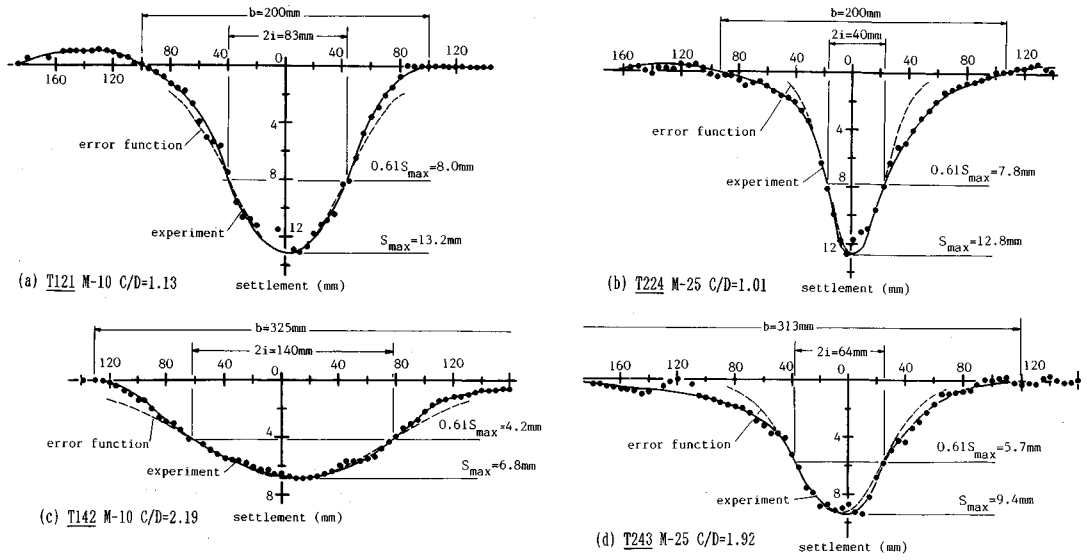

Fig. 14 Surface settlement profiles for two types of soils.

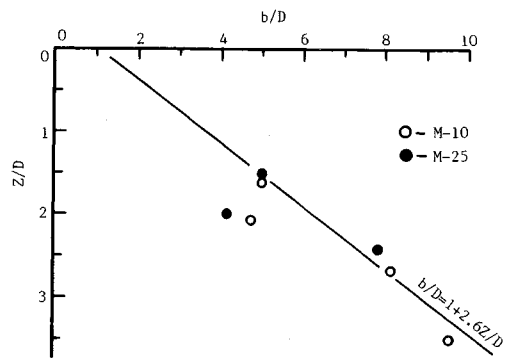

Fig. 15 Observed relationship between b/D and z/D.

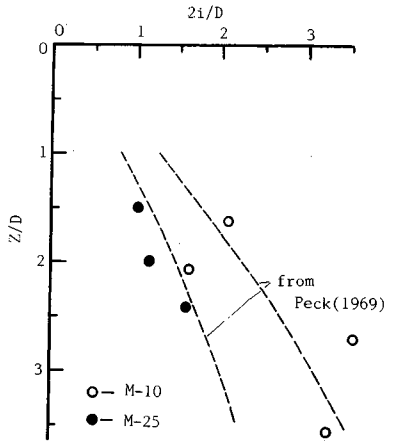

Fig. 16 Observed relationship between $2i/D$ and z/D.

almost linearly with z/D and is independent of the soil type up to 3.5 of z/D which is within the range of this tests. The best fit line is expressed by the equation

$$b/D=1+2.6\cdot z/D \quad \cdots\cdots (8)$$

The results of tests T135 and T236 are somewhat different from those for the other tests. As described before, the non-contact type displacement transducer was used for these tests in an attempt to measure the crown settlements. It is considered that this transducer has hampered the free deformations of soil around the tunnel, resulting in low values of b.

While b indicates the width of settlement troughs, $2i$ specifies the width of the area where large settlements occur. The ratio $2i/D$ represents the steepness of the settlement troughs. Observed values of $2i/D$ are plotted against z/D in Fig. 16. There is a marked difference between the results for the two different soils. The results for M-10 excluding test T135 are located close to the upper limit defined by Peck[1] and those for M-25 are along the lower limit. The ground loss calculated from the observed surface troughs is 100 % and 65 % of the initial cross sectional area of the tunnel for M-10 and M-25 respectively. This implies that further settlements could have developed for M-25 and it is possible that the actual values of i are higher than those listed in Table 4. The theoretical ground loss can be obtained by integrating Equation (7) within $\sqrt{2\pi}\,iS_{max}$. From this it is understood that the increase of i during the process of the ground loss reaching 100 % of the tunnel area is at most 50 %. This increase in i, however, does not change the overall trend in the relationship between $2i/D$ and z/D that the settlement troughs for M-25 are steeper than those for M-10. This is consistent with the results of the upper bound calculation. As shown in Fig. 13, M-10 with higher strength anisotropy has a larger collapse area than M-25 with lower anisotropy, giving rise to a similar conclusion that the area in which large settlements occur is larger for M-10 than for M-25.

4. CONCLUSIONS

Following conclusions are drawn from the study based on centrifuge model tests and upper bound calculations on the stability of two-dimensional shallow tunnels in normally consolidated clay.

(1) The undrained stability of unlined tunnels increases with increasing tunnel cover-to-diameter ratios. No significant difference on the relationship between the stability ratio and the cover-to-diameter ratio was obtained from the model tests on two soils.

(2) Failure is due to extension in soil mass above the tunnel followed by downward movements of this block of soil.

(3) The upper bound calculation in which strength anisotropy is taken into account provides a reasonable prediction for the stability of unlined tunnels.

(4) The pore pressure drops sharply in the vicinity where a tunnel collapses.

(5) Observed deformations compare well with those in the collapse mechanism obtained from the upper bound calculation. The soil mass above the tunnel moves almost vertically downwards and soil that is slightly away from the tunnel tends to move towards the tunnel at a small angle.

(6) The error functions obtained using the values of S_{max} and $2i$ compare fairly well with observed profiles of the surface settlement especially near the centre-line of tunnels, where S_{max} and $2i$ are the maximum surface settlement and the distance between two inflection points.

(7) The profile of the surface settlements of plastic soil with low strength anisotropy becomes steeper than less plastic soil with high strength anisotropy, although the width of surface settlements for identical cover-to-diameter ratios is almost the same irrespective of soil type.

REFERENCES

1) Peck, B. B. : Deep excavations and tunnelling in soft ground, State of the art volume 7th ICSMFE, pp. 225-290, 1969.
2) Ward, W. H. and Pender, M. J. : Tunnelling in soft ground—general report, Proc. of 10th ICSMFE, Vol. 4, pp. 261-275, 1981.
3) Atkinson, J. H. and Potts, D. M. : Subsidence above shallow tunnels in soft ground, Jour. of GE Div., ASCE, Vol. 103, No. GT4, pp. 307-325, 1981.
4) Mair, R. J., Gunn, M. J. and O'Reilly, M. P. : Ground movements around shallow tunnels in soft clay, Proc. of 10th ICSMFE, Vol. 1, pp. 323~328, 1981.
5) Taylor, R. N. : Ground movements associated with tunnels and trenches, Ph. D. Thesis, Cambridge University, 1980.
6) Broms, B. B. and Bennermark, H. : Stability of clay at vertical openings, Jour. of SMFE Div., ASCE, Vol. 93, No. 10, pp. 71-94, 1967.
7) Kobayashi, T. : Studies of displacement in soft ground associated with shield tunnelling, Ph. D. Thesis, Tokyo University, 1982 (in Japanese).
8) Murayama, S. and Fujimoto, T. : Earth pressure on circular tunnel lining due to stress relaxation in visco-elastic ground, Proc. of JSCE, No. 205, pp. 93-106, 1972 (in Japanese).
9) Ito, T. and Hisatake, M. : Ground pressure acting on arbitrary shaped tunnel lining in visco-elastic ground, Proc. of JSCE, No. 307, pp. 51-57, 1981 (in Japanese).
10) Kimura, T. and Mair, R. J. : Centrifuge testing of model tunnels in soft clays, Proc. of 10th ICSMFE, Vol. 1, pp. 319-322, 1981.
11) Akagi, K. and Mori, A. : Effect of excavation ratio on the deformation of ground after tunnelling by shield, 40th Annual conference of JSCE, No. Ⅲ, pp. 337-338, 1985 (in Japanese).
12) Hanya, T. : Ground movements due to construction of shields-driven tunnel, Proc. of 9th ICSMFE, Case history volume, pp. 759-790, 1977.
13) Mair, R. J. : Centrifugal modelling of tunnel construction in clay, Ph. D. Thesis, Cambridge University, 1979.
14) Davis, E. H., Gunn, M. J., Mair, R. J. and Seneviratne, H. N. : The stability of shallow tunnels and underground openings in cohesive materials, Geotechnique, Vol. 30, No. 4, pp. 397-416, 1980.
15) Kimura, T., Kusakabe, O., Takemura, J. and Saitoh, K. : Preparation of a normally consolidated clay stratum in a centrifuge, Soils and Foundations, Vol. 24, No. 4, pp. 71-83, 1984.
16) Kusakabe, O. : Stability of excavations in soft clay, Ph. D. Thesis, Cambridge University, 1982.
17) For example, Kimura, T. and Saitoh, K. : Influence of strain rate on pore pressures in consolidated undrained shear tests on cohesive soils, Soils and Foundations, Vol. 23, No. 1, pp. 80-90, 1983.
18) Kimura, T., Nakase, A., Kusakabe, O., Saitoh, K. and Ohta, A. : Geotechnical centrifuge model tests at Tokyo Institute of Technology, Technical report No. 30, Dep. of Civil Engineering. T. I. T., pp. 7-33, 1984.
19) Nakase, A. and Kamei, T. : Undrained shear strength anisotropy of normally consolidated cohesive soils, Soils and Foundations, Vol. 23, No. 1, pp. 91-101, 1983.
20) Glossop, N. H. and Farmer, I. W. : Settlement associated with removal of compressed air pressure during tunnelling in alluvial clay, Geotechnique, Vol. 29, No. 1, pp. 67-72, 1979.

(Received July 18 1989)